Spin-torque-induced switching and precession in fully epitaxial Fe/MgO/Fe magnetic tunnel junctions

Rie Matsumoto,[1,2,3,4] Akio Fukushima,[1] Kay Yakushiji,[1] Satoshi Yakata,[1] Taro Nagahama,[1] Hitoshi Kubota,[1] Toshikazu Katayama,[1] Yoshishige Suzuki,[1,2] Koji Ando,[1] Shinji Yuasa,[1] Benoit Georges,[4] Vincent Cros,[4] Julie Grollier,[4,*] and Albert Fert[4]

[1]*National Institute of Advanced Industrial Science and Technology (AIST), Nanoelectronics Research Institute, Tsukuba, Ibaraki 305-8568, Japan*

[2]*Graduate School of Engineering Science, Osaka University, 1-3 Machikaneyama, Toyonaka, Osaka 560-8531, Japan*

[3]*Japan Society for the Promotion of Science, Sumitomo-Ichibancho FS Bldg., 8 Ichibancho, Chiyoda-ku, Tokyo 102-8472, Japan*

[4]*Unité Mixte de Physique CNRS/Thales and Université Paris Sud 11, Route Départementale 128, 91767 Palaiseau, France*

(Received 8 August 2009; revised manuscript received 9 October 2009; published 12 November 2009)

We experimentally investigated current-driven oscillation in fully epitaxial Fe(001)/MgO(001)/Fe(001) magnetic tunnel junctions (MTJs) to pave the way for a better understanding of why the linewidth (a few hundred MHz) of microwave oscillation in spin-torque nano-oscillators (STNOs) based on textured MTJs is much larger than that (smaller than 10 MHz) in STNOs based on current-perpendicular-to-plane giant-magnetoresistance junctions. The epitaxial Fe/MgO/Fe STNO is a model system for studying the physics of spin-transfer torque because it has a well-defined single-crystal barrier and electrode layers with atomically flat interfaces. In the Fe/MgO/Fe STNOs, clear spin-torque-induced switching and spin-torque-induced precession were observed in epitaxial MTJs. When the initial magnetic alignment was antiparallel and the bias current exceeded the threshold current, a state in which the spin-torque compensates for the damping, the STNOs showed a rapid increase in the peak intensity, a redshift of the peak frequency, and a minimum linewidth, all clear evidence of spin-torque-induced precession above the threshold current. The minimum linewidth of the STNOs was 200 MHz, which is comparable to that of textured CoFeB/MgO/CoFeB MTJs. This indicates that the origin of the large linewidth cannot be attributed to structural inhomogeneity in textured MTJs. When the initial magnetic alignment was parallel, the microwave spectrum showed a single peak, which has rarely been observed in textured MTJs without application of a perpendicular magnetic field. The mechanism of the single-peak oscillation can be explained by taking account of the induced perpendicular magnetic anisotropy in the 3-nm-thick Fe(001) free layer grown on the MgO(001) barrier layer.

DOI: 10.1103/PhysRevB.80.174405 PACS number(s): 75.40.Gb, 73.40.Gk, 73.40.Rw, 85.75.−d

I. INTRODUCTION

A magnetic tunnel junction (MTJ) exhibits the tunneling magnetoresistance (TMR) effect.[1–3] The magnitude of the TMR is evaluated from the magnetoresistance (MR) ratio, which is defined as $(R_{AP}-R_P)/R_P \times 100(\%)$, where R_{AP} and R_P are the tunneling resistances when the magnetizations of the two electrodes are aligned antiparallel (AP) and parallel (P). First-principles theory predicted the giant TMR effect in fully epitaxial Fe/MgO/Fe MTJs with a crystalline MgO(001) barrier due to coherent spin-dependent tunneling of the fully spin-polarized Δ_1 states.[4,5] In accordance with this theory, giant MR ratios of up to 410% at room temperature (RT) have been experimentally achieved in fully epitaxial MTJs with a single-crystal MgO(001) barrier[6–9] and in polycrystalline MTJs with a textured MgO(001) barrier.[10] Moreover, a giant TMR effect of up to 600% at RT has been obtained in CoFeB/textured MgO(001)/CoFeB MTJs[11,12] in which the CoFeB electrode layers are amorphous in the as-grown state but crystallize in bcc(001) texture by post annealing.[13]

Because CoFeB/MgO/CoFeB MTJs are highly compatible with processes for manufacturing the read heads of hard disk drives and magnetic random memories,[13] this MTJ structure is the mainstream technology for device application. Spin-transfer torque[14–17] has also been experimentally investigated using CoFeB/MgO/CoFeB MTJs.[18–24] On the other hand, fully epitaxial MTJs with a single-crystal MgO(001) barrier are a model system for investigating the physics of spin-dependent tunneling transport because of their well-defined crystal structure and magnetic properties. In addition to the giant TMR effect, epitaxial MTJs exhibit various novel phenomena such as oscillation of the TMR with respect to the tunneling barrier thickness (t_{MgO}), an intrinsic interlayer exchange coupling mediated by spin-polarized tunneling electrons, and complex spin-dependent tunneling spectra.[7,13,25–30] However, there are no reports of epitaxial MTJs being used in experimental studies of spin-torque-induced phenomena.

The spin-transfer torque[14,15] in MTJs can induce various phenomena such as magnetization switching,[18–20] the spin-torque diode effect (spin-torque-induced ferromagnetic resonance),[21–23] and spin-torque-induced oscillation.[24] The nanosized MTJs for the oscillation experiments are called "spin-transfer nano-oscillators (STNOs)."[17,31] These experimental studies have been performed by using 100-nm-sized CoFeB/MgO/CoFeB MTJs. Although such MTJs are well suited for demonstrating the spin-torque-induced phenomena, the inhomogeneous crystalline structure of the textured MTJs makes it difficult to understand the detailed mechanism of the phenomena. One of the most fundamental questions is why the linewidth (a few hundred MHz) of spin-

torque-induced oscillation observed in CoFeB/MgO/CoFeB MTJs (Refs. 24, 32, and 33) and Al-O-based MTJs (Ref. 34) is much larger than that (smaller than 10 MHz) in current-perpendicular-to-plane giant-magnetoresistance (CPP-GMR) junctions.[17,31] This large linewidth is a serious problem for practical application of STNOs although the microwave power of MgO-based MTJs is more than 1000 times that of the CPP-GMR junctions.

Before this problem can be overcome, the origin of the large linewidth needs to be clarified. One possible origin is the spatial distribution of the bias dc current (I_{dc}) in the junction. In the case of the CPP-GMR junction whose spacer layer is metal, the current density (J) is almost homogeneous at any point in the junction even if the spacer layer is inhomogeneous. In an MTJ, on the other hand, the spacer layer is insulating. If the insulating tunnel barrier layer has an inhomogeneous thickness or crystal condition, the current density may be inhomogeneous, which can cause enhancement of the linewidth.

Fully epitaxial MTJs are suitable for clarifying whether the large linewidth originates from structural inhomogeneity in MTJs or from more intrinsic mechanisms, for the following reasons. In textured CoFeB/MgO/CoFeB MTJs, the MgO tunnel barrier layer has grain boundaries.[13,35] In fully epitaxial Fe/MgO/Fe(001) MTJs, on the other hand, the MgO(001) layer has a uniform single crystalline structure without grain boundaries, and the Fe(001)/MgO(001) interfaces are atomically flat.[7,36] Furthermore, textured CoFeB electrodes have spatial distribution of magnetocrystalline anisotropy while single-crystal Fe(001) electrodes have well-defined four-fold magnetocrystalline anisotropy. By exploiting the interplay between the magnetocrystalline anisotropy of Fe and the spin-transfer torque, Lehndorff *et al.*[37] investigated the angular dependences of CPP-GMR and spin-transfer torque.

For MgO-based MTJs to exhibit spin-torque-induced switching (ST switching) and precession (ST precession), they must have a high MR ratio and an ultralow resistance-area (*RA*) product. Such ultralow *RA* MTJs were originally developed for the read heads of hard disk drives. For textured CoFeB/MgO/CoFeB MTJs with an MgO thickness (t_{MgO}) of 1.02 nm (1.05 nm), Nagamine *et al.*[38] reported an ultralow *RA* of 0.4 $\Omega\ \mu m^2$, (1.1 $\Omega\ \mu m^2$), and a high MR ratio of 57% (119%) at RT. It should be noted here that the MTJ with a t_{MgO} of 1.02 nm exhibited mixed tunneling and metallic transport while the MTJ with a t_{MgO} of 1.05 nm exhibited clear tunneling transport.[39] Clarifying the basic transport properties before carrying out experiments on ST precession is therefore important.

In this paper, we report the first successful demonstrations of ST switching and ST precession in fully epitaxial Fe/MgO/Fe(001) STNOs having an ultralow *RA* product and discuss their detailed mechanisms. We first describe the basic transport properties of the MTJs in Sec. III A and discuss the t_{MgO} dependence of the transport mechanism. Then we describe and discuss the spin-torque-induced phenomena through *tunneling* transport in fully epitaxial Fe/MgO/Fe(001) STNOs in Sec. III B.

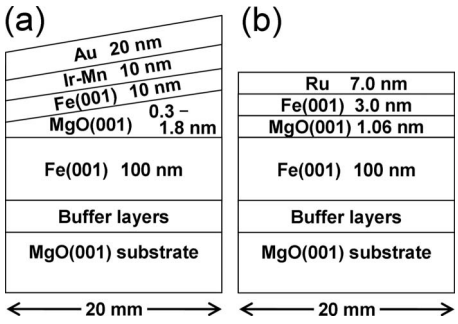

FIG. 1. Cross section of fully epitaxial magnetic tunnel junction (MTJ) films: (a) Fe/MgO/Fe MTJ for magnetotransport experiment and (b) Fe/MgO/Fe MTJ for spin-torque experiment.

II. EXPERIMENTAL

High-quality fully epitaxial Fe/MgO/Fe(001) MTJ films with an ultrathin MgO layer, grown using molecular beam epitaxy (MBE) growth, were fabricated into nanopillars using microfabrication techniques (electron-beam lithography and Ar-ion milling). In this section, we describe the fabrication of the epitaxial MTJs used for the (A) transport experiment and (B) spin-torque experiments.

A. Fully epitaxial MTJs with wedge-shaped ultrathin MgO(001) layer for transport experiment

Cross section of the MTJ films used for the transport experiment is shown schematically in Fig. 1(a). It had a wedge-shaped MgO layer and the layers up to the top bcc Fe(001) electrode were grown epitaxially on a MgO(001) single-crystal substrate. The high-quality ultrathin MgO(001) tunnel barrier was prepared on bcc Fe(001) using layer-by-layer epitaxial growth. The t_{MgO} was varied from 0.3 to 1.8 nm. Because the wedge-shaped MgO layer was grown on the same substrate, the relative experimental error in t_{MgO} between MTJs on the same substrate was negligibly small.[13] The growth conditions for the epitaxial bcc Fe/MgO/Fe MTJs were the same as previously reported.[7,25] In each MTJ, the Fe(001) top electrode was exchange biased by an antiferromagnetic Ir-Mn layer, which was deposited by rf sputtering at RT.

In the microfabrication process, the films were etched down to the bottom Fe(001) layer to form nanosized MTJs. The etching method used resulted in the junctions being slightly larger than designed owing to tapering of the side wall [see Fig. 4(a)]. The designed junction sizes was 200 nm$\times$400 nm, while the actual junction size after etching were 220 nm$\times$420 nm, as estimated from scanning electron microscopy images.

The MR ratio and *RA* product were measured using an ac four-probe method. The typical applied ac excitation was around 1 $mV_{p\text{-}p}$ at 97 kHz. The measured resistance of the MTJs included the parasitic resistance of the Au cap layer and Ir-Mn layer, which was serially connected to the net resistance of the MTJ. The estimated parasitic resistance was about 0.08 $\Omega\ \mu m^2$.

B. Fully epitaxial Fe/MgO/Fe MTJs for spin-torque experiment

A cross section of the MTJ film used in the spin-torque experiment is shown schematically in Fig. 1(b). The growth

conditions for the bottom Fe layer and MgO barrier layer were the same as described above. The top Fe layer (3.0 nm), which acts as a free layer of a pseudospin-valve MTJ, was grown at RT to prevent island growth on the MgO layer as much as possible. The 3-nm-thick Fe layer showed a square magnetic hysteresis loop, indicating the formation of a continuous Fe layer on the MgO [see Fig. 4(c)]. The MTJ film was microfabricated into STNOs with a nominal junction area of 50 nm$\times$150 nm (actual junction area of 70 nm $\times$170 nm) with the long sides along the Fe$\langle 100 \rangle$ easy axis. An external magnetic field (H_{ext}) was applied to the long side of the junction for the measurements described in Sec. III B. The temperature dependences of R_P and R_{AP} were measured using the dc two-probe method. The ST switching and precession properties were investigated at RT. In this paper, a positive bias means that electrons flow from the bottom electrode to the top electrode.

To evaluate the saturation magnetization (M_s) of the 3-nm-thick Fe grown on the MgO precisely, we also deposited fully epitaxial Cr(50 nm)/MgO(1.06 nm)/Fe(001) (3 nm)/Ru film on a MgO(001) substrate. We measured the magnetization curves of the film at RT by applying H_{ext} parallel and perpendicular to the film plane using a superconducting quantum interference device (SQUID) magnetometer and observed that its M_s was 1430 emu/cm^3. We also found that Fe(001) (3 nm) on MgO(001) has a perpendicular anisotropy (K_u) of 3.6×10^6 erg/cm^3 in addition to the shape anisotropy of the plain film (i.e., the effect of demagnetization energy). Note that the Fe layer is in-plane magnetized in a zero magnetic field because the shape anisotropy is larger than the induced K_u. The effect of the perpendicular anisotropy on spin-torque-induced oscillation is discussed in Sec. III B 2.

III. RESULTS AND DISCUSSION

A. Transport properties of fully epitaxial MTJs with ultrathin MgO(001) tunnel barrier

The t_{MgO} dependence of the *RA* product for the epitaxial Fe/MgO/Fe MTJs is plotted in Fig. 2(a). For $t_{MgO}>1.0$ nm, the *RA* product increased exponentially as a function of t_{MgO}, which is a characteristic of ideal tunnel junctions. The fitting to the exponential increment is represented by the dotted line. For 0.7 nm$<t_{MgO}<$1.0 nm, the *RA* product decreased more rapidly than the exponential decrease. For $t_{MgO}<0.5$ nm, the *RA* approached a constant value corresponding to the parasitic resistance noted above.

The t_{MgO} dependence of the MR ratio for the Fe/MgO/Fe(001) MTJs is plotted in Fig. 2(b). For 0.8 nm$<t_{MgO}<$1.0 nm, the MR ratio rapidly decreased. This corresponds to the rapid decrease in *RA* for $t_{MgO}<1.0$ nm. It should be noted, however, that the MR ratio took a local maximum at t_{MgO}=0.6 nm [indicated by the arrow in Fig. 2(b)], at which point a high MR ratio of up to 16% at RT and an ultralow *RA* of 0.19 $\Omega\ \mu m^2$ were obtained at the same time. The origin of the MR enhancement at $t_{MgO}\sim0.6$ nm is discussed in the next paragraph.

To investigate the transport mechanism at various t_{MgO}, we measured the temperature dependence of the *RA* product and MR ratio. The temperature dependence of the *RA* product for the P state is a good criterion for determining the transport mechanism. If the transport mechanism is tunneling, the *RA* product should be nearly independent of temperature or should decrease with increasing temperature. If metallic transport is dominant, the *RA* product should increase with temperature. For $t_{MgO}>1.0$ nm, the *RA* product for the P state was nearly independent of temperature, as shown in Fig. 4(b), clearly indicating that the transport mechanism was tunneling. For $t_{MgO}<1.0$ nm, on the other hand, the *RA* product increased with temperature while the MR ratio decreased with increasing temperature, as shown in Fig. 3. This indicates that metallic transport was dominant in these junctions. In the junctions with $t_{MgO}<1.0$ nm, the me-

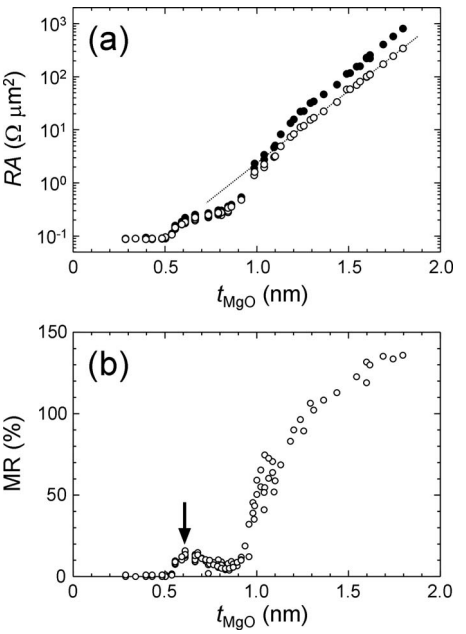

FIG. 2. (a) Dependence of resistance-area (*RA*) product and (b) MR ratio on thickness of MgO(001) barrier layer (t_{MgO}) for Fe/MgO/Fe MTJs at room temperature (RT). (a) Open and solid circles represent P and AP states, respectively. Dotted line represents linear relationship between t_{MgO} and log(*RA*) for P state. (b) Arrow indicates Fe/MgO/Fe MTJ with *RA* product of 0.19 $\Omega\ \mu m^2$ and MR ratio of 16%.

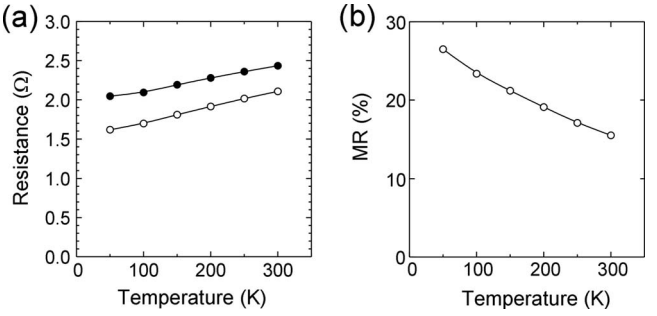

FIG. 3. Temperature dependence of (a) junction resistance and (b) MR ratio for Fe/MgO/Fe MTJ exhibiting *RA* product of 0.19 $\Omega\ \mu m^2$ and MR ratio of 16% at RT. Open and solid circles in (a) represent P and AP states, respectively.

tallic transport is considered to take place through locally conductive paths in the MgO layer. A previous investigation[36] of the local transport property of ultrathin MgO(001) layers by *in situ* scanning tunneling microscopy revealed that the MgO layer thinner than 4 monolayers (ML) shows a metallic transport property while that 4 or more ML thick acts as a tunnel barrier. A thickness of 1.0 nm corresponds to 4.7 ML, which is a mixture of 4- and 5-ML-thick MgO if the layer-by-layer growth of the MgO was perfect. Imperfect layer-by-layer growth results in spatial thickness variation, so there are points at which the MgO layer is thinner than 4 ML. Such points are considered to be the origin of the observed metallic transport for $t_{MgO} < 1.0$ nm. A junction with such a layer has locally conductive paths in the insulating layer and is called a "current-confined-path (CCP) current-perpendicular-to-plane (CPP) giant-magnetoresistance (GMR) junction."[40] The enhancement of MR at $t_{MgO} \sim 0.6$ nm is considered to be a similar effect as measured in CPP-GMR films with a CCP nano-oxide layer (NOL). It should be noted that, however, the observed MR ratio of 16% at the ultralow *RA* of 0.19 $\Omega\ \mu m^2$ is much higher than the MR ratios of conventional CCP-CPP-GMR junctions.[41] In this study, the MTJs with a t_{MgO} of 1.06 nm, which clearly exhibited tunneling transport, were used for the ST switching and precession experiments.

B. Spin-torque-induced phenomena in fully epitaxial MgO-based MTJs

1. Basic magnetotransport properties of STNOs

Typical values of the MR ratio and R_P of the fully epitaxial Fe/MgO/Fe STNOs fabricated on one substrate were respectively 90%–100% and 300–350 Ω at RT and a low bias voltage of +5 mV. The temperature dependence of the *RA* product shown in Fig. 4(b) clearly indicates that the transport mechanism was tunneling. A cross section of a STNO is shown schematically in Fig. 4(a). The bottom Fe electrode layer was intentionally overetched by about 1 to 2 nm. This resulted in a stray magnetic field around the bottom Fe electrode, which acted on the top Fe electrode; the effect of this field is explained later. Because the over etching was minimal, the bottom Fe layer remained a continuous film with a volume of 2 cm × 2 cm × 98–99 nm. This volume was significantly larger than that of the top Fe electrode (70 nm × 170 nm × 3 nm), so the magnetization of the bottom electrode was not affected by the stray field from the top Fe electrode or by the spin-transfer torque. The magnetization of the bottom electrode depended solely on the external magnetic field, H_{ext}. When an H_{ext} higher than the coercive field of the bottom electrode (~20 Oe) was applied along the in-plane easy axis of the electrode, its magnetization was aligned parallel to H_{ext}. The magnetization of the top electrode, on the other hand, was affected by other factors such as the stray field from the bottom electrode, the spin-transfer torque, and the in-plane demagnetization field due to the elliptical shape. Thus, the top electrode acted as a free layer in the ST switching and precession experiments.

The stray magnetic field from the bottom electrode acting on the top one was used to create the AP state at a low H_{ext}.

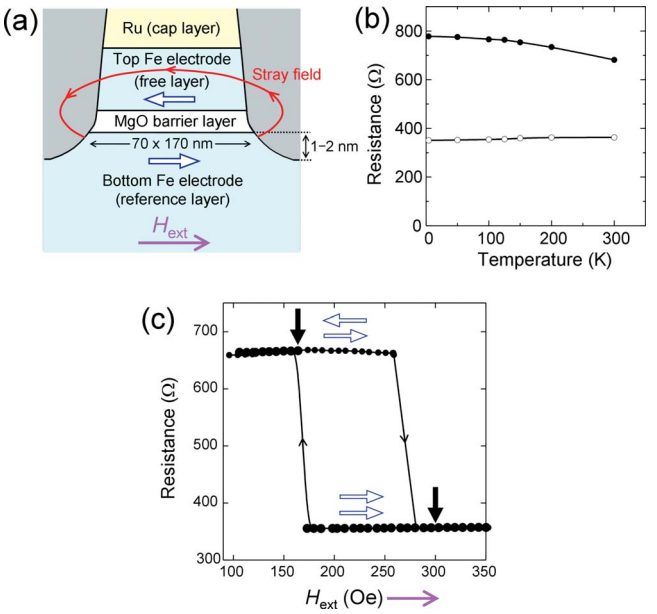

FIG. 4. (Color online) (a) Schematic illustration representing cross section of Fe/MgO/Fe STNO. Thick white arrows edged with blue represent magnetizations of top and bottom Fe layers. Thin purple arrow represents external magnetic field (H_{ext}). (b) Temperature dependence of junction resistance for Fe/MgO/Fe STNO for P state (open circles) and AP state (solid circles). (c) Minor hysteresis loop of Fe/MgO/Fe STNO measured at constant bias current (I_{dc}) of +100 μA at RT. Thick black arrows represent H_{ext} of +167 Oe and +301 Oe at which points ST precession experiment was conducted. Thick white arrows represent magnetic alignment of MTJ under application of H_{ext} the direction of which is represented by thin purple arrow.

The minor hysteresis loop of a STNO measured at a constant bias current of +100 μA and at RT is shown in Fig. 4(c). Under H_{ext} larger than 20 Oe as well as all over the range of H_{ext} shown in Fig. 4(c), the magnetization of the bottom electrode was always aligned parallel to H_{ext}. The minor loop of the top electrode showed a shift due to antiferromagnetic dipolar coupling between the top and bottom electrodes induced by the stray field. It should be noted that the top electrode showed the other minor hysteresis loop at around −200 Oe because the STNO was a pseudospin valve one without an exchange-bias layer. The magnetization loop was symmetric with respect to H_{ext}. In the spin-torque experiments, we used the minor loop in the positive range of H_{ext}.

2. ST precession

To determine whether the magnetization of the top electrode of the STNO was affected by the spin-transfer torque, we performed an ST switching experiment in which we measured the resistance (*R*)—pulse current (*I*) characteristics. To facilitate switching from the P to the AP state, we applied H_{ext}, which shifted from the center of the loop toward the switching field from the P state to AP state. The STNOs exhibited clear ST switching at pulse currents of −0.8 mA (I_{PtoAP}) and +0.8 mA (I_{APtoP}) and a pulse width (t_p) of 10 ms. We estimated the intrinsic switching current density (J_{c0}) and thermal stability factor ($\Delta = E/k_BT$; where *E* represents

the energy barrier that the magnetization of the free layer must overcome during magnetization reversal) by measuring the t_p dependence of the switching current density (J_c) and fitting the plots to the thermally activated model.[42–44] Typical values of the J_{c0} and Δ of the fully epitaxial Fe/MgO/Fe STNOs fabricated on the same substrate were 2×10^7 A/cm^2 and 30, respectively. The J_{c0} of the Fe/MgO/Fe(001) MTJs is larger than that of CoFeB/MgO/CoFeB MTJs having the same free layer thickness because the M_s of 3-nm-thick Fe (1430 emu/cm^3) is larger than that of 3-nm-thick CoFeB (~1100 emu/cm^3).[18] After measuring these switching properties in each MTJ fabricated on the same substrate, we conducted an ST precession experiment.

For an H_{ext} of +167 Oe [indicated by thick black arrow in Fig. 4(c)], where the initial MTJ state is AP, the STNO exhibited ST precession. A typical microwave spectrum is shown in the inset of Fig. 5(a). When the initial state was AP, the spectrum showed a main peak and small satellite peaks. The main peak is considered to be a center mode, which corresponds to the precession at the center of an elliptical junction.[24,32] The small satellite peaks are considered to be edge modes, which have been observed in textured CoFeB/MgO/CoFeB MTJs.[24,32]

Figure 5 shows the bias current dependence of (a) the peak intensity, (b) frequency, and (c) linewidth of the center mode. In the AP state, application of a positive I_{dc} resulted in (a) a significant increase in the peak intensity, (b) a significant redshift of the peak frequency, and (c) a local minimum of the linewidth, all clear evidence of ST precession above the threshold current (I_{th}).[45] The I_{th} above which ST precession takes place can be estimated from the current at which the linewidth extrapolates to zero because the spin-torque compensates for the damping.[24,45] In this STNO exhibiting the properties shown in Fig. 5, I_{th} was estimated to be $+0.88 \pm 0.32$ mA. The regime below I_{th} where the linewidth decreases linearly is associated with thermally excited ferromagnetic resonance (TE-FMR) noise.[45] The minimum linewidth of the fully epitaxial STNOs was 200 MHz, which is comparable to that of textured CoFeB/MgO/CoFeB MTJs.[24,32]

For an H_{ext} of +301 Oe [indicated by thick black arrow in Fig. 4(c)], where the initial MTJ state is P, the STNO exhibited a slightly different behavior. A typical microwave spectrum is shown in the inset of Fig. 6(a). The single peak is attributed to homogeneous oscillation inside the Fe(001) free layer. The single-peak oscillation for the initial P state was very reproducible. It was observed for all H_{ext} and all bias currents at which oscillation took place. It should be noted here that such a single-peak spectrum has rarely been observed in textured CoFeB/MgO/CoFeB MTJs unless a perpendicular magnetic field was applied.[24,32]

Figure 6 shows the bias current dependence of (a) the peak intensity, (b) frequency, and (c) linewidth of the single peak. In the P state, application of a negative I_{dc} resulted in (a) an increase in the peak intensity, (b) a redshift of the peak frequency, and (c) a decrease in the linewidth. In the initial P state, however, we did not observe a clear threshold for ST precession because the applied current was smaller than I_{th}. The measured spectra are related to TE-FMR enhanced by spin-torque.[34] Extrapolation of the linewidth—I_{dc} relationship resulted in an estimated I_{th} of -4.3 ± 0.7 mA. This large threshold current I_{th} observed in the P state mainly originates from the fact that in this case the applied H_{ext} of +301 Oe inhibits the magnetization motion (while in the case of the AP state H_{ext}=+167 Oe favors magnetization dynamics) as can be seen in Fig. 4(c). The linewidth for the initial P state was also comparable to that of textured CoFeB/MgO/CoFeB MTJs.[24,32]

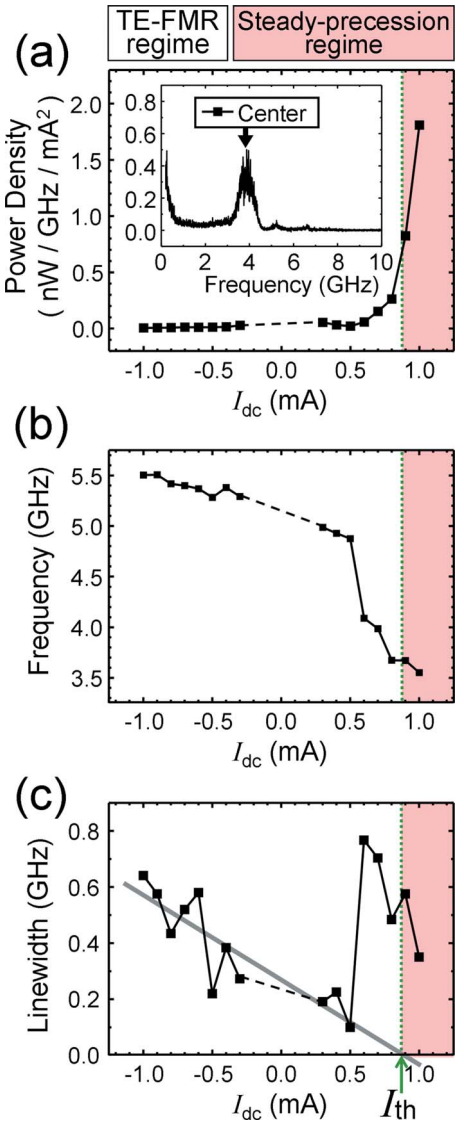

FIG. 5. (Color online) Current-driven oscillation and spin-torque-induced precession in Fe/MgO/Fe STNO at in-plane H_{ext}=+167 Oe where initial state of MTJ is AP. I_{dc} dependence of (a) peak intensity, (b) frequency, and (c) linewidth. Inset in (a) is microwave spectrum at I_{dc}=+0.80 mA. Gray line in (c) is linear extrapolation of linewidth used to evaluate threshold current (I_{th}). Colored area above I_{th} represents spin-torque-induced precession (ST precession) regime and unpigmented area below I_{th} represents TE-FMR regime.

These results clearly indicate that the origin of the large linewidth cannot be attributed to structural inhomogeneity in textured MTJs. In all-metallic devices, smaller linewidths have been measured (<10 MHz). It is therefore a key point to understand the difference between the MTJs and metallic

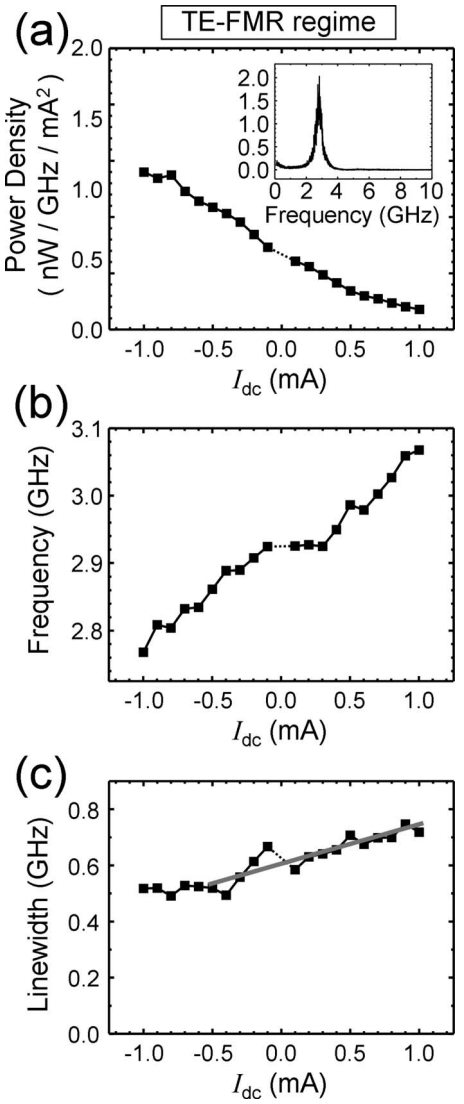

FIG. 6. Current-driven oscillation in Fe/MgO/Fe MTJ at in-plane H_{ext}=+301 Oe where initial state of MTJ is P. Bias current dependence of (a) peak intensity, (b) frequency, and (c) linewidth. Inset in (a) is the microwave spectrum at I_{dc}=−0.80 mA. Gray line in (c) is a linear extrapolation of linewidth used to evaluate I_{th}. The data shown in Fig. 6 are in TE-FMR regime.

systems that gives rise to these very distinct coherence times. The possible origins of the large linewidth are discussed below. First, MR ratio in MTJs is much larger than in metallic systems. Therefore, significant spatial fluctuations of the current and/or its spin polarization can generate an additional magnetic noise through the spin-transfer torque. This decoherence mechanism is expected to be larger at low temperature where the TMR ratio is also larger. It has been recently demonstrated by studying the temperature dependence of the linewidth in CoFeB/MgO/CoFeB that this effect is not predominant.[33] This latest study has also shown that a spin-torque-induced white noise generates magnetization chaotization. Second, the large linewidths observed in epitaxial MgO MTJs definitely rule out the effect of the spatial inhomogeneities of the current paths as the major source of chaos. The last main difference between spin-transfer oscillators based on MTJs and metallic systems is the amplitude of the injected I_{dc}. In metallic devices, a large I_{dc} is injected, creating a strong Oersted field, which plays a key role in the selection of the excited mode.[46] The low Oersted field in MTJs is unable to pin the magnetization at the edges of the junction, possibly inducing complex dynamics of the magnetic system and incoherent magnetic modes. Recently, spin-transfer-induced vortex oscillations in MTJs showing low linewidths (~1 MHz) have been reported.[47] In this case, the vortex mode is stabilized by the circular shape of the free layer and by the Oersted field. This latest result, proving that the linewidth is particularly mode dependent, supports the conclusion that the large linewidths related to uniform magnetization precessions in MTJs find their origin in the chaotization of this mode.

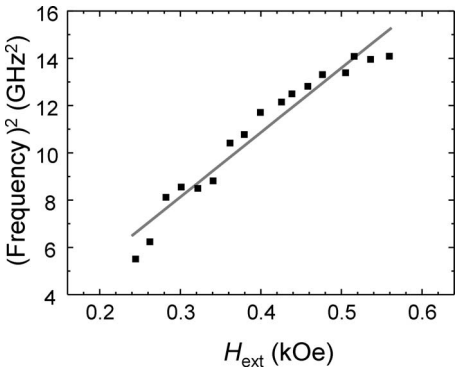

FIG. 7. Dependence of TE-FMR peak frequency on in-plane H_{ext} in Fe/MgO/Fe STNO for P state measured at I_{dc}=+0.30 mA. Gray line is least-squares fitting to Eq. (1)

The origin of the observed single-peak oscillation is discussed below. A similar single-peak oscillation has been observed when a perpendicular magnetic field was applied to textured CoFeB/MgO/CoFeB MTJs.[48] A perpendicular magnetic field is considered to reduce the effect of the distribution of the demagnetization field (H_d) in the free layer, so the free layer is considered to generate the single-mode oscillation. As mentioned in Sec. II B, a 3-nm-thick Fe free layer grown on a MgO(001) barrier layer has a relatively large perpendicular magnetic anisotropy (K_u) of 3.6×10^6 erg/cm^3. Because this K_u is still smaller than the shape anisotropy of the free layer, which is $-2\pi M_s^2 = -1.2 \times 10^7$ erg/cm^3, the free layer exhibits in-plane magnetization. If the effect of this perpendicular anisotropy on ST precession was equivalent to that of a perpendicular field, the observed single-peak oscillation would be explained by the same mechanism. To clarify the effect of perpendicular anisotropy, we investigated the H_{ext} dependence of the TE-FMR peak frequency (f). The H_{ext} dependence of f^2 is shown in Fig. 7. The plot points were fitted to the Kittel formula [Eq. (1)].[49]

$$f^2 = \frac{\gamma_{Fe}^2}{4\pi^2}(\boldsymbol{H}_{ext} + \boldsymbol{H}_d - \boldsymbol{H}_{perp})(\boldsymbol{H}_{ext} + \boldsymbol{H}_{shift})$$

$$\sim \frac{\gamma_{Fe}^2}{4\pi^2}(\boldsymbol{H}_d - \boldsymbol{H}_{perp})(\boldsymbol{H}_{ext} + \boldsymbol{H}_{shift}). \quad (1)$$

The γ_{Fe}, H_{ext}, H_{perp}, and H_{shift} denote respectively the gyromagnetic ratio of Fe at RT ($\gamma_{Fe}/2\pi=2.926$ GHz/kOe),[49,50] the in-plane external field, the perpendicular anisotropy field induced by K_u, and the in-plane stray magnetic field from the bottom Fe layer. For $H_{perp}=0$, which corresponds to zero perpendicular anisotropy, the fitting yields unreasonably small H_d and M_s ($H_d=4\pi M_s$) of 3.2 kOe and 250 emu/cm^3, respectively. Fitting the plot points to the Kittel formula by taking account of the perpendicular magnetic anisotropy gives reasonable H_d and M_s of 11 kOe and 900 emu/cm^3, respectively. Although this M_s is still smaller than the M_s obtained by SQUID measurement (1430 emu/cm^3), the difference is considered to be mainly due to the reduced demagnetizing factor because of the microstructuring[51] and the experimental error in K_u. Thus, the perpendicular anisotropy is considered to have the same effect as a perpendicular magnetic field and thus produce single-mode oscillation. As an origin of perpendicular anisotropy, the uniaxial strain associated with the epitaxial growth of Fe(001) on MgO(001) can be considered because the lattice mismatch of 3.6% is not negligibly small. Another possible origin of perpendicular anisotropy is the interfacial coupling between O and Fe orbitals.[52] However, the detailed mechanism of the induced perpendicular anisotropy is not clear at present.

IV. SUMMARY

We investigated spin-torque-induced oscillation in fully epitaxial Fe(001)/MgO(001)/Fe(001) MTJs to identify the origin of the large linewidth of microwave oscillation in STNOs based on MTJs. We fabricated fully epitaxial Fe/MgO/Fe MTJ film with t_{MgO} of 1.06 nm into STNOs with a lateral size of 70 nm$\times$170 nm. The STNOs exhibited clear tunneling transport with a MR ratio of 90%–100% and a junction resistance of 300–350 Ω for P state at RT. The 3-nm-thick top Fe electrode of the STNO acted as a free layer while the 100-nm-thick bottom Fe electrode acted as a reference layer. Clear ST switching in epitaxial MTJs was observed. The J_{c0} and Δ were estimated to be 2×10^7 A/cm^2 and 30, respectively. The epitaxial STNOs also exhibited ST precession. When the bias current exceeded the I_{th}, the STNOs showed a rapid increase in the peak intensity, a redshift of the peak frequency and a minimum of the linewidth, all clear evidence of ST precession above the I_{th}. The minimum linewidth of fully epitaxial STNOs was 200 MHz, which is comparable to that of textured CoFeB/MgO/CoFeB MTJs. This indicates that the origin of the large linewidth cannot be attributed to structural inhomogeneity in textured MTJs. When the initial magnetic alignment was P state, the spectrum showed a single peak, which has rarely been observed in textured MTJs unless a perpendicular magnetic field was applied. The mechanism of the single-peak oscillation can be explained by taking account of the induced perpendicular magnetic anisotropy in the 3-nm-thick Fe(001) free layer grown on the MgO(001) barrier layer.

ACKNOWLEDGMENTS

This work was supported in part by NEDO spintronics nonvolatile functionality project and JSPS KAKENHI (Grant No. 19·01159). We would like to thank Takayuki Seki, Etsuko Usuda, Mie Yamamoto, and Hidekazu Saito of AIST for their help with microfabrication of the samples, the *R-I* measurement and the magnetization measurement.

*Corresponding author; julie.grollier@thalesgroup.com

[1] M. Jullière, Phys. Lett. **54A**, 225 (1975).
[2] J. S. Moodera, L. R. Kinder, T. M. Wong, and R. Meservey, Phys. Rev. Lett. **74**, 3273 (1995).
[3] T. Miyazaki and N. Tezuka, J. Magn. Magn. Mater. **139**, L231 (1995).
[4] W. H. Butler, X.-G. Zhang, T. C. Schulthess, and J. M. MacLaren, Phys. Rev. B **63**, 054416 (2001).
[5] J. Mathon and A. Umerski, Phys. Rev. B **63**, 220403(R) (2001).
[6] S. Yuasa, A. Fukushima, T. Nagahama, K. Ando, and Y. Suzuki, Jpn. J. Appl. Phys., Part 2 **43**, L588 (2004).
[7] S. Yuasa, T. Nagahama, A. Fukushima, Y. Suzuki, and K. Ando, Nat. Mater. **3**, 868 (2004).
[8] S. Yuasa, T. Katayama, T. Nagahama, A. Fukushima, H. Kubota, Y. Suzuki, and K. Ando, Appl. Phys. Lett. **87**, 222508 (2005).
[9] S. Yuasa, A. Fukushima, H. Kubota, Y. Suzuki, and K. Ando, Appl. Phys. Lett. **89**, 042505 (2006).
[10] S. S. P. Parkin, C. Kaiser, A. Panchula, P. M. Rice, B. Hughes, M. Samant, and S.-H. Yang, Nat. Mater. **3**, 862 (2004).
[11] D. D. Djayaprawira, K. Tsunekawa, M. Nagai, H. Maehara, S. Yamagata, N. Watanabe, S. Yuasa, and K. Ando, Appl. Phys. Lett. **86**, 092502 (2005).
[12] S. Ikeda, J. Hayakawa, Y. Ashizawa, Y. M. Lee, K. Miura, H. Hasegawa, M. Tsunoda, F. Matsukura, and H. Ohno, Appl. Phys. Lett. **93**, 082508 (2008).
[13] S. Yuasa and D. D. Djayaprawira, J. Phys. D **40**, R337 (2007).
[14] J. Slonczewski, J. Magn. Magn. Mater. **159**, L1 (1996).
[15] L. Berger, Phys. Rev. B **54**, 9353 (1996).
[16] E. B. Myers, D. C. Ralph, J. A. Katine, R. N. Louie, and R. A. Buhrman, Science **285**, 867 (1999).
[17] S. I. Kiselev, J. C. Sankey, I. N. Krivorotov, N. C. Emley, R. J. Schoelkopf, R. A. Buhrman, and D. C. Ralph, Nature (London) **425**, 380 (2003).
[18] H. Kubota, A. Fukushima, Y. Ootani, S. Yuasa, K. Ando, H. Maehara, K. Tsunekawa, D. D. Djayaprawira, N. Watanabe, and Y. Suzuki, Jpn. J. Appl. Phys., Part 2 **44**, L1237 (2005); Appl. Phys. Lett. **89**, 032505 (2006).
[19] J. Hayakawa, S. Ikeda, Y. M. Lee, R. Sasaki, T. Meguro, F. Matsukura, H. Takahashi, and H. Ohno, Jpn. J. Appl. Phys. **44**, L1267 (2005).
[20] Z. Diao, D. Apalkov, M. Pakala, Y. Ding, A. Panchula, and Y. Huai, Appl. Phys. Lett. **87**, 232502 (2005).
[21] A. A. Tulapurkar, Y. Suzuki, A. Fukushima, H. Kubota, H. Maehara, K. Tsunekawa, D. D. Djayaprawira, N. Watanabe, S. Yuasa, Nature (London) **438**, 339 (2005).
[22] H. Kubota, A. Fukushima, K. Yakushiji, T. Nagahama, S. Yuasa,

K. Ando, H. Maehara, Y. Nagamine, K. Tsunekawa, D. D. Djayaprawira, N. Watanabe, and Y. Suzuki, Nat. Phys. **4**, 37 (2008).
[23] J. C. Sankey, Y. T. Cui, J. Z. Sun, J. C. Slonczewski, R. A. Buhrman, and D. C. Ralph, Nat. Phys. **4**, 67 (2008).
[24] A. M. Deac, A. Fukushima, H. Kubota, H. Maehara, Y. Suzuki, S. Yuasa, Y. Nagamine, K. Tsunekawa, D. D. Djayaprawira, and N. Watanabe, Nat. Phys. **4**, 803 (2008).
[25] R. Matsumoto, A. Fukushima, T. Nagahama, Y. Suzuki, K. Ando, and S. Yuasa, Appl. Phys. Lett. **90**, 252506 (2007).
[26] J. Faure-Vincent, C. Tiusan, C. Bellouard, E. Popova, M. Hehn, F. Montaigne, and A. Schuhl, Phys. Rev. Lett. **89**, 107206 (2002).
[27] T. Katayama, S. Yuasa, J. Velev, M. Ye. Zhuravlev, S. S. Jaswal, and E. Y. Tsymbal, Appl. Phys. Lett. **89**, 112503 (2006).
[28] Y. Ando, T. Miyakoshi, M. Oogane, T. Miyazaki, H. Kubota, K. Ando, and S. Yuasa, Appl. Phys. Lett. **87**, 142502 (2005).
[29] S. Nishioka, R. Matsumoto, H. Tomita, T. Nozaki, Y. Suzuki, H. Itoh, and S. Yuasa, Appl. Phys. Lett. **93**, 122511 (2008).
[30] R. Matsumoto, A. Fukushima, K. Yakushiji, S. Nishioka, T. Nagahama, T. Katayama, Y. Suzuki, K. Ando, and S. Yuasa, Phys. Rev. B **79**, 174436 (2009).
[31] W. H. Rippard, M. R. Pufall, S. Kaka, S. E. Russek, and T. J. Silva, Phys. Rev. Lett. **92**, 027201 (2004).
[32] D. Houssameddine, S. H. Florez, J. A. Katine, J.-P. Michel, U. Ebels, D. Mauri, O. Ozatay, B. Delaet, B. Viala, L. Folks, B. D. Terris, and M.-C. Cyrille, Appl. Phys. Lett. **93**, 022505 (2008).
[33] B. Georges, J. Grollier, V. Cros, A. Fert, A. Fukushima, H. Kubota, K. Yakushijin, S. Yuasa, and K. Ando, Phys. Rev. B **80**, 060404(R) (2009).
[34] S. Petit, C. Baraduc, C. Thirion, U. Ebels, Y. Liu, M. Li, P. Wang, and B. Dieny, Phys. Rev. Lett. **98**, 077203 (2007).
[35] M. Mizuguchi, Y. Suzuki, T. Nagahama, and S. Yuasa, Appl. Phys. Lett. **91**, 012507 (2007).
[36] M. Mizuguchi, Y. Suzuki, T. Nagahama, and S. Yuasa, Appl. Phys. Lett. **88**, 251901 (2006).
[37] R. Lehndorff, M. Buchmeier, D. E. Bürgler, A. Kakay, R. Hertel, and C. M. Schneider, Phys. Rev. B **76**, 214420 (2007).
[38] Y. Nagamine, H. Maehara, K. Tsunekawa, D. D. Djayaprawira, N. Watanabe, S. Yuasa, and K. Ando, Appl. Phys. Lett. **89**, 162507 (2006).
[39] H. Maehara *et al.* (unpublished).
[40] M. A. M. Gijs, S. K. J. Lenczowski, and J. B. Giesbers, Phys. Rev. Lett. **70**, 3343 (1993).
[41] H. Fukuzawa, H. Yuasa, and H. Iwasaki, J. Phys. D **40**, 1213 (2007).
[42] R. H. Koch, J. A. Katine, and J. Z. Sun, Phys. Rev. Lett. **92**, 088302 (2004).
[43] Z. Li and S. Zhang, Phys. Rev. B **69**, 134416 (2004).
[44] K. Yagami, A. A. Tulapurkar, A. Fukushima, and Y. Suzuki, Appl. Phys. Lett. **85**, 5634 (2004).
[45] J.-V. Kim, Q. Mistral, C. Chappert, V. S. Tiberkevich, and A. N. Slavin, Phys. Rev. Lett. **100**, 167201 (2008).
[46] I. N. Krivorotov, D. V. Berkov, N. L. Gorn, N. C. Emley, J. C. Sankey, D. C. Ralph, and R. A. Buhrman, Phys. Rev. B **76**, 024418 (2007).
[47] J. Grollier, V. Cros, B. Georges, A. Dussaux, C. Deranlot, A. Fert, A. V. Khvalkovskiy, K. A. Zvezdin, G. Faini, A. Fukushima, H. Kubota, K. Yakushijin, S. Yuasa, and K. Ando, The International Conference on Magnetism, Karlsruhe, Germany, 2009 (unpublished), Paper No. We-FW7-01.
[48] T. Wada *et al.* (unpublished).
[49] C. Kittel, *Introduction to Solid State Physics*, 7th ed. (Wiley, New York, 1996), p. 505.
[50] A. J. P. Meyer and G. Asch, J. Appl. Phys. **32**, S330 (1961).
[51] Y. Suzuki and H. Kubota, J. Phys. Soc. Jpn. **77**, 031002 (2008).
[52] A. Manchon, C. Ducruet, L. Lombard, S. Auffret, B. Rodmacq, B. Dieny, S. Pizzini, J. Vogel, V. Uhlíř, M. Hochstrasser, and G. Panaccione, J. Appl. Phys. **104**, 043914 (2008).